Energy materials

Room-temperature, all-solid-state lithium metal batteries enabled by a moderate-temperature formation method

Fuming Du[1],* , Ting Liao[2], Tuo Ye[1], Yuanzhi Wu[1], Gang Guo[3], Ke Zhu[4], Haibin Wang[4], Yong Zhang[3], and Zhongxiang Xie[3]

[1] *Research Institute of Automobile Parts Technology, Hunan Institute of Technology, Hengyang 421002, People's Republic of China*
[2] *Hunan Institute of Scientific and Technical Information, Changsha 410001, People's Republic of China*
[3] *School of Science, Hunan Institute of Technology, Hengyang 421002, People's Republic of China*
[4] *School of Materials Science and Engineering, Hunan Institute of Technology, Hengyang 421002, People's Republic of China*

ABSTRACT

Poor electrode/solid electrolyte interface contacts and interface stabilities limit the normal operation and practical applications of all-solid-state lithium metal batteries (ASSLMBs) at room temperature. Herein, a facile, moderate-temperature formation method was described to improve the interface between the garnet-type solid electrolyte and electrode material, giving ASSLMBs good electrochemical performance, even at room temperature (25 °C). During this moderate-temperature formation method, the ASSLMBs were charged/discharged once at 100 °C. Consequently, the interface impedance between the Li metal anode and garnet-type solid electrolyte decreased, but more importantly, this method formed a stable interface with higher ionic conductivity between the LiFePO$_4$ composite cathode and garnet-type solid electrolyte via the decomposition of Li$_2$CO$_3$ between the cathode and solid electrolyte. Therefore, the total internal resistance of the ASSLMBs was reduced by half at 25 °C compared with after simply heating at 100 °C. The discharge capacity at 0.05 C and 25 °C increased from 20 to 120 mAh g^{-1}, and the batteries showed a stable cyclability of 100 cycles with 99% Coulombic efficiency. The moderate-temperature formation method was beneficial to promote the application of room temperature, all-solid-state batteries.

Introduction

The organic liquid electrolytes used in conventional lithium-ion batteries have problems such as flammability, prone to leakage, and high voltage intolerance [1]. All-solid-state lithium metal batteries based on solid electrolytes can solve these problems, because solid electrolytes are essentially safer, but can also increase the operating voltage of the batteries [2–4]. Moreover, their high hardness can also block the growth of lithium dendrites, which is helpful for the application of lithium metal anodes, thereby simultaneously improving battery safety and energy density [5]. Currently, ceramic-based solid electrolytes are considered good candidates to replace organic liquid electrolytes. Examples of ceramic-based solid electrolytes include perovskites (e.g., $Li_xLa_{2/3-x/3}TiO_3$), NASICON (e.g., $Li_{1.3}Al_{0.3}Ti_{1.7}(PO_4)_3$, $Li_{1+x}Al_xGe_{2x}(PO_4)_3$), thio-LISICON (e.g., $Li_{10}GeP_2S_{12}$), halide electrolytes (e.g., Li_3YCl_6), cubic garnet-type $Li_7La_3Zr_2O_{12}$ (LLZO), and their variants [6–9]. Among these, Ta-doped garnet $Li_7La_3Zr_2O_{12}$ (LLZTO) has received widespread attention due to its high room-temperature lithium-ion conductivity ($> 1.0 \times 10^{-3}$ S cm^{-1}), high lithium-ion transfer number (≈ 1), and high oxidation stability (> 5 V vs Li/Li^+), as well as good chemical/electrochemical stability to lithium metal [10–14].

Nevertheless, the performances of all-solid-state lithium metal batteries based on LLZTO have been inhibited by high interface impedances [15–17]. The interface contacts between the stiff solid electrolyte and the solid electrode can be categorized as insufficient point contacts at the micro-level, and since solid electrolytes cannot immerse into and "wet" the electrode as effectively as liquid electrolytes, this led to difficulties in Li^+ transport inside the electrode (especially the cathode) and across the interface between the electrode and the solid electrolyte [18–20]. Moreover, studies have shown that garnet-type solid electrolytes, such as LLZTO, were prone to form Li_2CO_3 or LiOH with low Li^+ conductivity and lithiophobicity on the surface when encountering CO_2 or H_2O in the air, which increased the interface impedance [21–25]. There are many methods to improve the interface between the lithium metal anode and LLZTO solid electrolyte [15]. For example, the wettability between the lithium metal anode and the LLZTO interface can be significantly improved by using heat (> 700 °C) or acid treatments to obtain a clean LLZTO surface. Thin-film processing or chemical reactions can also be used to form ion/electron/ion–electron hybrid conductors (such as Al_2O_3, ZnO_2, Mg, Sn, $Li_3N + Cu$) as an artificial interlayer on the LLZTO surface, thereby reducing the interface impedance between the lithium metal anode and the LLZTO solid electrolyte [26–31].

However, the cathode/LLZTO interface impedance still does not have a good solution because both the cathode and the cathode/LLZTO interface require fast ion and/or electron conduction channels. Conventional methods include adding a layer of flexible polymer electrolyte or a small amount of liquid electrolyte at the interface. The low ionic conductivity of the former makes it difficult for operation at room temperature, while the latter sacrifices battery safety and is not suitable for large-scale applications [32–34]. By constructing a porous LLZO/dense LLZO double-layer electrolyte structure and adding $Li_4Ti_5O_{12}$, LLZO, C, and poly(vinylidene fluoride) (PVdF) to the porous LLZO layer, this can help increase Li^+ transport at the $Li_4Ti_5O_{12}$/LLZO interface, but there has been no report on the electrochemical performance of the solid-state batteries at room temperature [35]. Although the $LiCoO_2$/LLZO interface impedance was reduced by co-firing $LiCoO_2$, LLZO, Li_3BO_3, or $Li_{2.3}C_{0.7}B_{0.3}O_3$ at high temperatures (> 700 °C), the battery capacity was small at room temperature (~ 94 mAh g^{-1}) [36]. At the same time, the intercalation and de-intercalation of Li^+ caused the volume of the cathode to change, and the cycle performance declined. Therefore, it is still challenging to address the issue using a facile method under mild conditions.

In our previous research, to build a mixed ion–electron conduction channel in the cathode, "Polymer-in-salt" electrolyte was used as a binder and Ketjen Black carbon as a conductive agent in a $LiFePO_4$ cathode to reduce the composite cathode/LLZTO solid electrolyte interface impedance by increasing the concentration of lithium salt [37]. The $LiFePO_4$-based, all-solid-state lithium metal batteries had excellent performance at 60 °C but still did not work at room temperature. Herein, a simple and moderate-temperature (100 °C) formation method has been developed, namely, charging and discharging the solid batteries once at 100 °C, which was similar to the formation process of liquid lithium-ion batteries. As a result, the room-temperature

performances (25 °C) of all-solid-state lithium metal batteries were significantly improved, and the discharge capacity at 0.05 C was increased to 120 mAh g^{-1} with little reduction after 100 cycles.

Experimental

Synthesis of the garnet-type solid electrolytes

The garnet-structured $Li_{6.4}La_3Zr_{1.4}Ta_{0.6}O_{12}$ (LLZTO) ceramic electrolyte powders were synthesized using a conventional solid-state reaction method and sintered to form dense ceramics by hot-pressing technology. More details about the LLZTO synthesis and characterizations can be found in our previous work [37]. Then, LLZTO ceramics were processed into ceramic membranes with a thickness of 0.1 cm and a diameter of 1 cm. The LLZTO membranes were stored in an Ar-filled glove box with oxygen and moisture levels below 0.1 ppm.

Preparation of the composite cathodes and assembly of the solid-state batteries

Composite cathodes consisted of poly(vinylidene fluoride) (PVdF) (Alfa Aesar), $Li(CF_3SO_2)_2$ N (LiTFSI) (99.95%, Sigma-Aldrich), Ketjen Black (KB, Alfa Aesar) and home-made carbon-coated $LiFePO_4$ (LFP). The PVdF polymers were dissolved in N-methyl-2 pyrrolidone (NMP, Alfa Aesar) and stirred for 24 h, which were followed by additions of LiTFSI, LFP, and KB in an agate mortar and ground for 1 h. The LiTFSI was pre-baked at 80 °C in a vacuum for 48 h. The obtained slurries were blade coated on one side of the LLZTO ceramic membrane, then dried in an oven at 80 °C for 2 h to remove NMP. After being pressed with a stainless-steel plate, the cathodes were dried in a vacuum oven at 80 °C for an additional 12 h to remove the trace amounts of NMP and moisture. The typical mass of each cathode was approximately 2 mg. The weight ratios between LFP, LiTFSI, KB, PVdF were fixed at 50:35:10:5 according to the optimum ratio. Li foil was attached on the other side of the LLZTO ceramic membrane using high pressure in the Ar-filled glove box. Finally, each laminated, all-solid-state, lithium metal battery (LFP cathode/LLZTO/Li) was assembled in a Swagelok-type cell. Stainless-steel (SS) foils were chosen as current collectors, instead of Al foils, to avoid the reaction between Al and the PVdF: LiTFSI. The Li/LLZTO/Li and SS/LFP cathode/SS symmetrical batteries were also assembled in a similar method.

Characterization and electrochemical measurements

The cross-sectional morphologies of the LLZTO ceramic electrolyte/ LFP cathode interface were determined using a scanning electron microscope (SEM, FEI Magellan 400). The surface structure of LLZTO ceramic membranes and pure Li_2CO_3 samples were characterized by Fourier transform infrared spectrum (FTIR, Tenser 27, Bruker). Galvanostatic charging and discharging behaviors of the LFP cathode/LLZTO/Li batteries were investigated using an Arbin BT-2000 battery tester with the potential ranging from 4.0 to 2.76 V at 25 °C. Three pre-treatment processes were performed on the batteries before testing: (1) Rested at room temperature ($\sim$ 25 °C) for 6 h, (2) Heated at 100 °C in a thermostatic oven for 6 h, and then rested at 25 °C for 6 h, (3) Heated at 100 °C in a thermostatic oven for 6 h, then charged and discharged once at 100 °C and 0.1 C, and finally rested at 25 °C for 6 h. The current density was normalized to the mass of LFP as well as the area of the electrode, i.e.: 1 C being 170 mA g^{-1} or 200 mA cm^{-2}. The cycle and rate performance were tested after the process of (3). Electrochemical impedance spectroscopy (EIS) measurements were performed using a frequency range of 1 MHz to 0.1 Hz with a 10 mV amplitude using an Autolab instrument at either 25 or 100 °C.

Results and discussion

The schematic illustration of the LFP cathode/ LLZTO/Li battery is shown in Fig. 1a. The LFP cathodes consisted of $LiFePO_4$ (active material), PVdF: LiTFSI (polymer electrolyte), and C (conducting additive). Figure 1b shows that the interface between the LFP cathode and the LLZTO ceramic solid electrolyte was closely contacted with the help of the PVdF: LiTFSI. This contact led to solid batteries exhibited excellent electrochemical performance at 60 °C and 100 °C [37].

Figure 1 (**a**) Schematic illustration of the all-solid-state lithium metal battery (LFP cathode/LLZTO/Li); (**b**) SEM image of the interface contact zone between the LFP cathode and the LLZTO ceramic solid electrolyte.
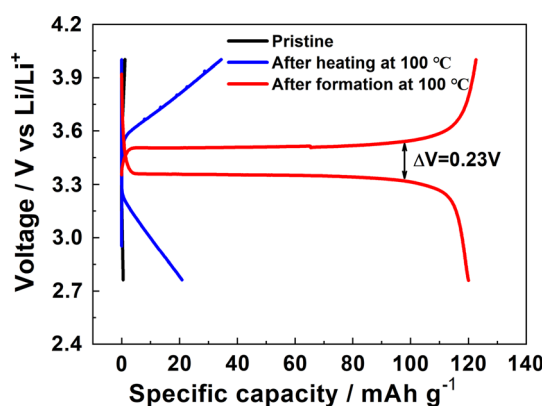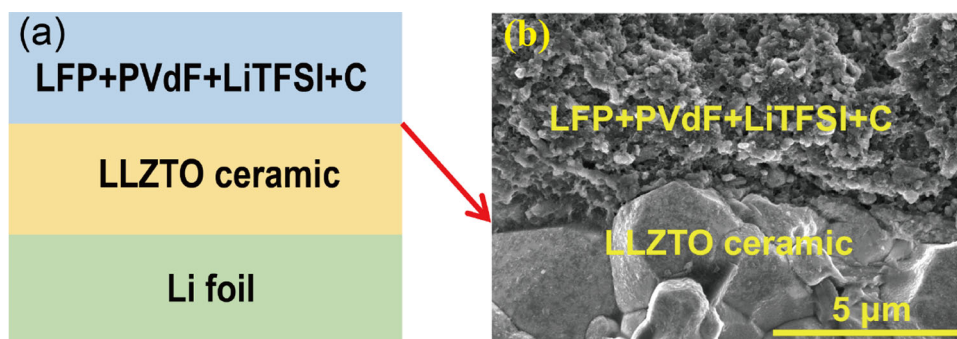
Figure 2 The first charge/discharge curve of LFP cathode/LLZTO/Li batteries under different conditions at 25 °C and 0.05 C, including the pristine state, after heating at 100 °C, and after formation at 100 °C.

Figure 2 compares the first charge/discharge curves of the all-solid-state lithium metal batteries under different conditions at 25 °C and 0.05 C. The charge/discharge polarization was very large in the pristine state as the all-solid-state lithium metal batteries were assembled and rested at room temperature (25 °C). The batteries cannot be charged or discharged normally, and the charge/discharge capacities were both almost 0. Since heating can improve the interface contact of solid-state batteries and may reduce the interface impedance, pristine batteries were heated at 100 °C for 6 h, then cooled down at 25 °C, and then charged/discharged at 25 °C. The all-solid-state lithium metal batteries can be charged/discharged at this time, but the polarization was still large, and the charge/discharge capacity did not exceed 40 mAh g^{-1}, which was far less from the theoretical capacity of LiFePO$_4$ (170 mAh g^{-1}). Finally, pristine batteries were charged and discharged once at 100 °C, then cooled down to 25 °C, and then charged and discharged again at 25 °C. It was surprising that the charge/

discharge capacities of the all-solid-state lithium metal batteries were substantially improved. The charge/discharge capacities were 123 and 120 mAh g^{-1}, respectively. The Coulombic efficiency was 97.6%, and the total over-potential was only 0.23 V (Fig. 2). The first charge/discharge cycle at a moderate temperature of 100 °C activated the battery at 25 °C, which was very similar to the formation process of the commercial liquid lithium-ion batteries [38]. After the commercial liquid lithium-ion batteries were prepared, they must be charged and activated with a small current before they can operate normally. During this formation process, lithium ions in the cathode de-intercalate and move into the graphite anode. The organic solvents (such as ethylene carbonate (EC), dimethyl carbonate (DMC)) and/or additives (such as vinylene carbonate (VC), fluoroethylene carbonate (FEC)) in the liquid electrolytes decomposed on the surface of the graphite anode. At the same time, a robust solid electrolyte interface (SEI) film was formed at the electrolyte/anode interface to improve the cycle and rate performance of the lithium-ion batteries [39–41]. Therefore, the first charge/discharge of the all-solid-state lithium metal batteries at 100 °C was denoted as moderate-temperature formation, which will activate the all-solid-state batteries at 25 °C.

Figure 3a shows the cycle performance of LFP cathode/LLZTO/Li batteries at 25 °C after moderate-temperature formation at 100 °C. After 100 cycles at 0.05 C, the capacity attenuation was small. The capacity fluctuation was due to temperature fluctuation, and the Coulombic efficiency was close to 99%. Although the capacity was lower than at 60 °C, the cycle performance was close, which suggested stable interfaces between the electrodes (cathode or anode) and the LLZTO solid electrolyte. The rate performance at 25 °C after moderate-temperature

Figure 3 (**a**) The cycle performance of discharge capacity and Coulombic efficiency at 0.05 C and (**b**) the rate performance of LFP cathode/LLZTO/Li batteries at 25 °C after moderate-temperature formation.
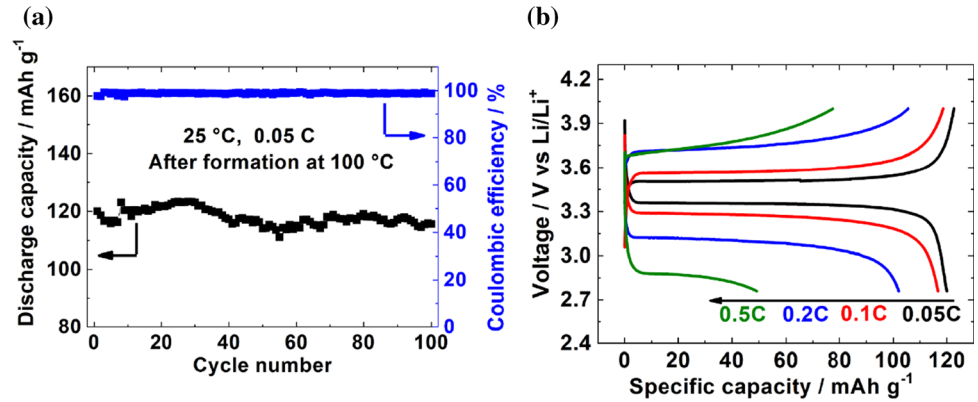
formation was shown in Fig. 3b. The discharge capacities of 0.1 C, 0.2 C, and 0.5 C were 117, 102, 49 mAh g^{-1}, respectively. This meant that the performance of 0.1 C was close to the performance at 0.05 C, but the charge/discharge capacity under high current (0.5 C) sharply decreased. Meanwhile, the charge/discharge polarization noticeably increased, and the total over-potential at 0.5 C was about 1 V.

Previous studies have indicated that increasing the working temperature of solid-state lithium metal batteries can improve their performance because high temperatures can reduce the interface impedance and improve the transport kinetics of both Li$^+$ and e^- [42]. As shown in Fig. 4a, the first discharge capacity of LFP cathode/LLZTO/Li batteries at 100 °C and 0.1 C was 138 mAh g^{-1}, much larger than at 25 °C (Fig. 2). The reason was that the total impedance of the batteries at 100 °C was much smaller than at 25 °C (pristine state), reducing by more than two orders of magnitude, shown in Fig. 4b. However, surprisingly, the charging curve had a very flat slope when the voltage was higher than 3.8 V vs. Li/Li$^+$, which was different from the redox platform of LiFePO$_4$ (3.4 V vs. Li/Li$^+$), resulting in a charging capacity

significantly higher than the discharge capacity. When the voltage reached 4.0 V, the first charging capacity reached 281 mAh g^{-1} with a large irreversible capacity (143 mAh g^{-1}), and the first Coulombic efficiency was lower than 50%. This situation was similar to the formation of an SEI film on the anode side, due to the decomposition of the electrolyte during the formation process of the liquid lithium-ion batteries, but there is a big difference. In the all-solid-state lithium metal batteries, the side reactions mainly take place on the cathode side. Our previous research on carbon electrodes has shown that KB and LiTFSI have side reactions at 60 °C and voltages above 4 V vs. Li/Li$^+$, leading to the accumulation of Li$_2$CO$_3$ in the cathode and an increase in the total impedance of LiNi$_{1/3}$Co$_{1/3}$Mn$_{1/3}$ cathode/ LLZTO/Li batteries [43]. On the contrary, at the higher temperature of 100 °C, both the Li$_2$CO$_3$ on the surface of LLZTO ceramic membranes, which is confirmed by FTIR for LLZTO even stored in glove box (shown in Fig. 5) and the Li$_2$CO$_3$ by-product (shown in Ref [43]) formed due to side reactions may decompose to form Li$_2$O (Li$_2$CO$_3$ → 2Li$^+$ + 2e^- + 1/2O$_2$ + CO$_2$(E^0 = 3.82V/vsLi/Li$^+$)), which had

Figure 4 (**a**) The first charge and discharge curves of LFP cathode/LLZTO/Li batteries at 100 °C and 0.1 C; (**b**) The electrochemical impedance spectra (EIS) of pristine batteries at 25 °C and 100 °C. The inset shows the amplified EIS at 100 °C.
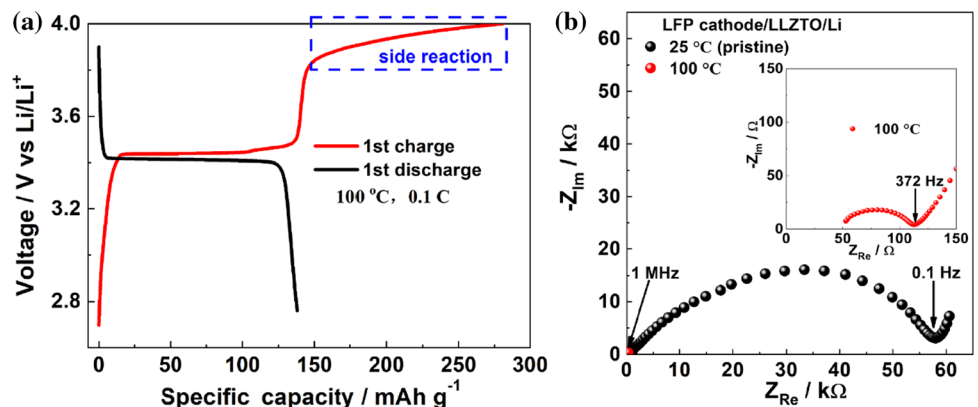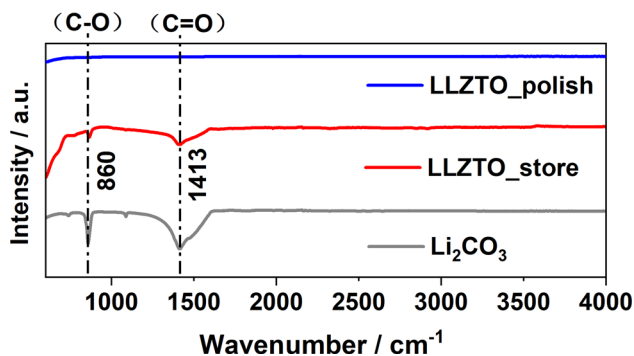
Figure 5 (**a**) FTIR spectra of the surface of LLZTO ceramic membranes and Li_2CO_3 samples, LLZTO_polish denotes LLZTO measured timely after polishing and LLZTO_store denotes LLZTO measured after storing in the Ar-filled glove box for at least 12 h.

better lithium-ion conductivity than Li_2CO_3, improving the interface contact between the LLZTO solid electrolyte and the $LiFePO_4$ cathode. As a result, when the LFP cathode/LLZTO/Li batteries were brought to room temperature (25 °C) after formation at 100 °C, the room-temperature charge and discharge capacities were significantly improved (Fig. 2).

Similar phenomena about the decomposition of Li_2CO_3 have been reported in both solid-state lithium batteries and lithium-ion batteries [22, 25, 44]. Li_2CO_3 can be used as an electrolyte additive to improve the performance of liquid lithium-ion batteries at relatively high temperatures (40 °C) compared to relatively low temperatures (20 °C) [45]. Recently, Delluva et al. have proved the electrochemical

Figure 6 (**a**) Electrochemical impedance spectra (EIS) of LFP/LLZTO/Li all-solid-state lithium metal batteries measured at 25 °C after heating or formation at 100 °C; (**b**) The best equivalent circuit to describe the EIS in (**a**); (**c**) EIS of Li/LLZTO/Li symmetrical batteries at 25 °C (after heating at 100 °C); (**d**) EIS of SS/LFP cathode/SS symmetrical batteries at 25 °C (after heating at 100 °C).
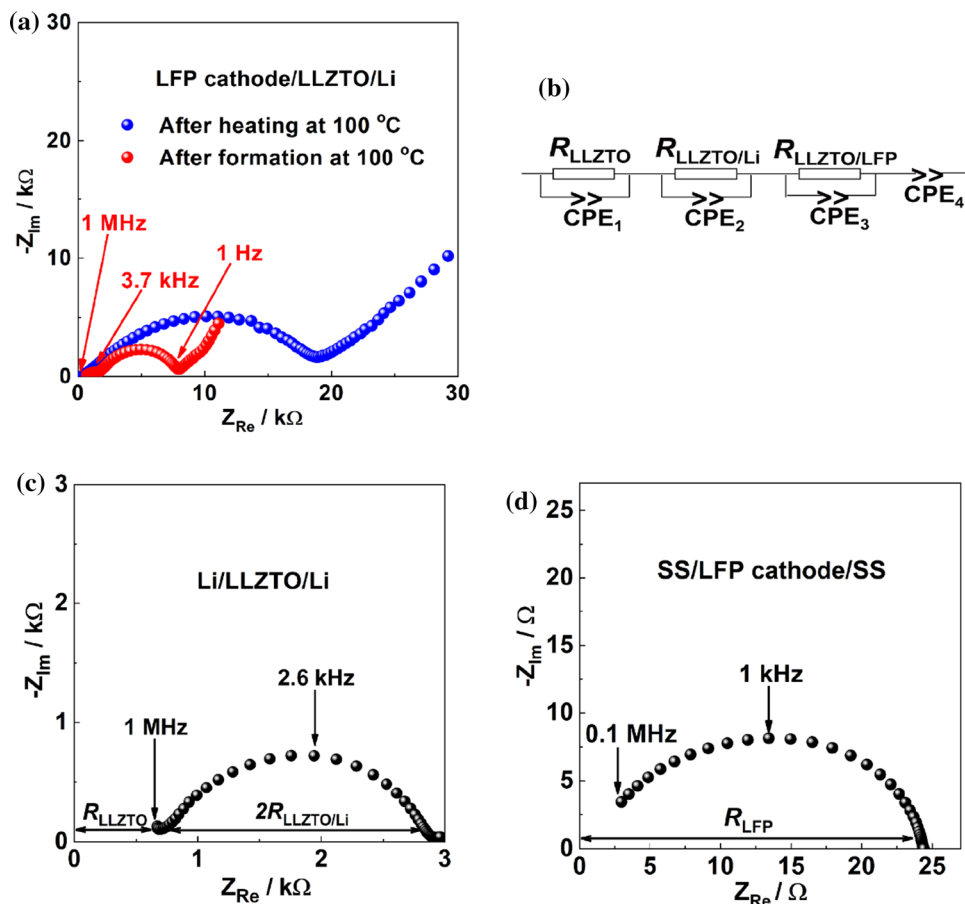
decomposition of interfacial Li_2CO_3 (between cathode/LLZTO interface) in thin-film garnet cells (LMO/LLZTO/Li and Au/LLZTO/Li) and confirmed that gas (CO_2 and O_2) evolution was specifically from the cathode interface at charging potentials > 3.8 V (vs Li/Li$^+$) by operando electrochemical mass spectrometry (EC–MS) [46]. However, the total impedance of their garnet cells (discharged state) was slightly increased after the electrochemical decomposition of interfacial Li_2CO_3, which is contrary to our results (discussed below). The reason could be that the high temperature (100 °C) will benefit to the move of flexible polymer electrolyte (PVdF:LiTFSI) in the LFP cathodes and within the cathode/LLZTO interface, consequently, the flexible polymer electrolyte (with higher Li$^+$ conductivity) will fill gaps caused by the decomposition of Li_2CO_3 timely, which will avoid the delamination between cathode/LLZTO interface (occurred in thin-film garnet cells) and finally decrease the interfacial impedance of LFP cathode/LLZTO/Li batteries after formation.

To uncover the reason why the moderate-temperature formation method greatly improved the room-temperature performance of all-solid-state lithium metal batteries, Fig. 6a shows the electrochemical impedance spectra (EIS) of LFP cathode/LLZTO/Li batteries at room temperature (25 °C) after heating or formation at 100 °C. Compared with the pristine LFP cathode/LLZTO/Li batteries, when the batteries were only heated at 100 °C and then cooled back to 25 °C, the total impedance of the batteries was reduced by 2/3, from the pristine $\sim$ 60 kΩ (Fig. 4b) to $\sim$ 20 kΩ (Fig. 6a), but it is still large. On the other hand, after formation at 100 °C and then cooling back to 25 °C, the total impedance of the LFP cathode/LLZTO/Li batteries was further reduced by more than half compared with after heating at 100 °C, and the total impedance was less than 10 kΩ ($\sim$ 8 kΩ). That is why the room-temperature performance was distinct in Fig. 2. Figure 6b shows the best equivalent circuit of the LFP cathode/LLZTO/Li batteries, which can be deconvoluted into three major parts: (1) the resistance of the LLZTO ceramic solid electrolyte (R_{LLZTO}), (2) the interfacial resistance between LLZTO and Li anode ($R_{LLZTO/Li}$), (3) the interfacial resistance between LLZTO and LFP cathode ($R_{LLZTO/LFP}$). It is well known that heating at 100 °C can soften the Li metal and help improve the interface contact between the Li metal anode and the LLZTO solid

electrolyte, which was also true for the formation at 100 °C. Figure 6c shows the EIS of a Li/LLZTO/Li symmetrical battery at 25 °C after heating at 100 °C. The sum of the LLZTO solid electrolyte impedance ($R_{LLZTO} \approx 0.6$ kΩ) and the LLZTO/Li interface impedance ($R_{LLZTO/Li} \approx 1.1$ kΩ) was about 1.7 kΩ, which only accounts for 1/10 of the total impedance of the LFP cathode/LLZTO/Li battery after heating at 100 °C. Therefore, in this situation, the interface impedance ($R_{LLZTO/LFP}$) resulting from the interface between LLZTO and LFP cathode, including the interfaces within the LFP composite cathode, was large at room temperature. This was the dominant factor for charging and discharging all-solid-state lithium metal batteries at room temperature. Figure 6d shows that the interface impedance within the LFP composite cathode (R_{LFP}) was less than 25 Ω at room temperature due to the construction of Li$^+$ and e^- conducting channels in the cathode. The key became how to reduce the interface impedance between the LLZTO solid electrolyte and LFP cathode. Therefore, it can be inferred that the interface impedance between the LLZTO solid electrolyte and the LFP cathode was significantly reduced after formation at 100 °C, which was in agreement with the side reactions in Fig. 4a. This led to the smaller total impedance and better electrochemical performance of the LFP cathode/LLZTO/Li batteries at room temperature compared with after heating at 100 °C.

Conclusions

In summary, the moderate-temperature (100 °C) formation method enabled all-solid-state lithium metal batteries based on the garnet-type, LLZTO ceramic solid electrolyte to have good performance at room temperature (25 °C). Simple moderate-temperature heating improved the interface contact between the lithium metal and the LLZTO solid electrolyte but did not decrease the interface impedance between the composite cathode and the solid electrolyte. EIS proved that the latter was the dominant factor hindering the room-temperature operation of all-solid-state lithium metal batteries. By using the moderate-temperature formation method, Li_2CO_3 may decompose between the LFP composite cathode and the LLZTO solid electrolyte during the first charge, forming a more conductive interface, which included Li_2O. The impedance between the LFP composite

cathode and the LLZTO solid electrolyte was further reduced, and ultimately the room-temperature performance of the all-solid-state lithium metal batteries was greatly improved. At 25 °C, the all-solid-state batteries showed an initial specific discharge capacity of 120 mAh g^{-1} at 0.05 C and worked stably for 100 cycles with 99% Coulombic efficiency. The discharge capacities at 0.1 C, 0.2 C, and 0.5 C were 117, 102, 49 mAh g^{-1}, respectively. The performance under the large current rates needed to be further improved. The moderate-temperature formation method can be extended to other solid-state batteries using oxide solid electrolytes, which was beneficial to reduce the room-temperature interface impedance between the electrode and the solid electrolyte.

Acknowledgements

Declarations

Conflict of interest These authors declare no conflict of interest.

References

[1] Goodenough JB, Kim Y (2011) Challenges for rechargeable batteries. J Power Sour 196(16):6688–6694

[2] Jia M, Zhao N, Huo H, Guo X (2020) Comprehensive investigation into garnet electrolytes toward application-oriented solid lithium batteries. Electrochem Energy Rev 3(4):656–689. https://doi.org/10.1007/s41918-020-00076-1

[3] Manthiram A, Yu X, Wang S (2017) Lithium battery chemistries enabled by solid-state electrolytes. Nat Rev Mater 2(4):16103. https://doi.org/10.1038/natrevmats.2016.103

[4] Janek J, Zeier WG (2016) A solid future for battery development. Nat Energy 1(9):16141. https://doi.org/10.1038/nenergy.2016.141

[5] Zhao N, Khokhar W, Bi ZJ, Shi C, Guo XX, Fan LZ, Nan CW (2019) Solid garnet batteries. Joule 3(5):1190–1199. https://doi.org/10.1016/j.joule.2019.03.019

[6] Chen LK, Huang YF, Ma JB, Ling HJ, Kang FY, He YB (2020) Progress and perspective of all-solid-state lithium batteries with high performance at room temperature. Energy Fuels 34(11):13456–13472. https://doi.org/10.1021/acs.energyfuels.0c02915

[7] He LC, Oh JAS, Chua JJJ, Zhou HH (2021) Synthesis and interface modification of oxide solid-state electrolyte-based all-solid-state lithium-ion batteries: advances and perspectives. Func Mater Lett. https://doi.org/10.1142/s1793604721300024

[8] Hou MJ, Liang F, Chen KF, Dai YN, Xue DF (2020) Challenges and perspectives of NASICON-type solid electrolytes for all-solid-state lithium batteries. Nanotechnology. https://doi.org/10.1088/1361-6528/ab5be7

[9] Wang ZK, Liu J, Wang MF, Shen XW, Qian T, Yan CL (2020) Toward safer solid-state lithium metal batteries: a review. Nanoscale Adva 2(5):1828–1836. https://doi.org/10.1039/d0na00174k

[10] Xu LQ, Li JY, Deng WT, Shuai HL, Li S, Xu ZF, Li JH, Hou HS, Peng HJ, Zou GQ, Ji XB (2021) Garnet Solid electrolyte for advanced all-solid-state Li batteries. Adv Energy Mater. https://doi.org/10.1002/aenm.202000648

[11] Wang CW, Fu K, Kammampata SP, Mcowen DW, Samson AJ, Zhang L, Hitz GT, Nolan AM, Wachsman ED, Mo YF, Thangadurai V, Hu LB (2020) Garnet-type solid-state electrolytes: materials, interfaces, and batteries. Chem Rev 120(10):4257–4300. https://doi.org/10.1021/acs.chemrev.9b00427

[12] Kim A, Woo S, Kang M, Park H, Kang B (2020) Research progresses of garnet-type solid electrolytes for developing all-solid-state Li batteries. Front Chem. https://doi.org/10.3389/fchem.2020.00468

[13] Samson AJ, Hofstetter K, Bag S, Thangadurai V (2019) A bird's-eye view of Li-stuffed garnet-type Li7La3Zr2O12 ceramic electrolytes for advanced all-solid-state Li batteries. Energ Environ Sci 12(10):2957–2975. https://doi.org/10.1039/c9ee01548e

[14] Thangadurai V, Narayanan S, Pinzaru D (2014) Garnet-type solid-state fast Li ion conductors for Li batteries: critical review. Chem Soc Rev 43(13):4714–4727. https://doi.org/10.1039/c4cs00020j

[15] Yang LJ, Lu ZL, Qin YX, Wu C, Fu CK, Gao YZ, Liu J, Jiang L, Du ZY, Xie ZY, Li ZQ, Kong FD, Yin GP (2021) Interrelated interfacial issues between a Li7La3Zr2O12-

based garnet electrolyte and Li anode in the solid-state lithium battery: a review. J Mater Chem A 9(10):5952–5979. https://doi.org/10.1039/d0ta08179e

[16] Wang DW, Zhu CB, Fu YP, Sun XL, Yang Y (2020) Interfaces in garnet-based all-solid-state lithium batteries. Adv Energy Mater. https://doi.org/10.1002/aenm.202001318

[17] Kim KJ, Rupp JLM (2020) All ceramic cathode composite design and manufacturing towards low interfacial resistance for garnet-based solid-state lithium batteries. Energ Environ Sci 13(12):4930–4945. https://doi.org/10.1039/d0ee02062a

[18] Li JH, Wang RG (2021) Recent advances in the interfacial stability, design and in situ characterization of garnet-type Li7La3Zr2O12 solid-state electrolytes based lithium metal batteries. Ceram Int 47(10):13280–13290. https://doi.org/10.1016/j.ceramint.2021.02.034

[19] Balasubramaniam R, Nam CW, Aravindan V, Eum D, Kang K, Lee YS (2021) Interfacial engineering in a cathode composite based on garnet-type solid-state Li-ion battery with high voltage cycling. Chem Electro Chem 8(3):570–576. https://doi.org/10.1002/celc.202001116

[20] Huang J, Liang F, Hou MJ, Zhang YJ, Chen KF, Xue DF (2020) Garnet-type solid-state electrolytes and interfaces in all-solid-state lithium batteries: progress and perspective. Appl Mater Today. https://doi.org/10.1016/j.apmt.2020.100750

[21] Yang Y-N, Li Y-X, Li Y-Q, Zhang T (2020) On-surface lithium donor reaction enables decarbonated lithium garnets and compatible interfaces within cathodes. Nat Commun 11(1):5519. https://doi.org/10.1038/s41467-020-19417-1

[22] Huo H, Luo J, Thangadurai V, Guo X, Nan C-W, Sun X (2020) Li2CO3: a critical issue for developing solid garnet batteries. ACS Energy Lett 5(1):252–262. https://doi.org/10.1021/acsenergylett.9b02401

[23] Sharafi A, Yu S, Naguib M, Lee M, Ma C, Meyer HM, Nanda J, Chi M, Siegel DJ, Sakamoto J (2017) Impact of air exposure and surface chemistry on Li–Li7La3Zr2O12 interfacial resistance. J Mater Chem A 5(26):13475–13487. https://doi.org/10.1039/C7TA03162A

[24] Xia W, Xu B, Duan H, Tang X, Guo Y, Kang H, Li H, Liu H (2017) Reaction mechanisms of lithium garnet pellets in ambient air: the effect of humidity and CO2. J Am Ceram Soc 100(7):2832–2839

[25] Cheng L, Crumlin EJ, Chen W, Qiao R, Hou H, Franz Lux S, Zorba V, Russo R, Kostecki R, Liu Z, Persson K, Yang W, Cabana J, Richardson T, Chen G, Doeff M (2014) The origin of high electrolyte–electrode interfacial resistances in lithium cells containing garnet type solid electrolytes. PCCP 16(34):18294–18300. https://doi.org/10.1039/C4CP02921F

[26] Sharafi A, Kazyak E, Davis AL, Yu S, Thompson T, Siegel DJ, Dasgupta NP, Sakamoto J (2017) Surface chemistry mechanism of ultra-low interfacial resistance in the solid-state electrolyte Li7La3Zr2O12. Chem Mater 29(18):7961–7968. https://doi.org/10.1021/acs.chemmater.7b03002

[27] Huo H, Chen Y, Zhao N, Lin X, Luo J, Yang X, Liu Y, Guo X, Sun X (2019) In-situ formed Li2CO3-free garnet/Li interface by rapid acid treatment for dendrite-free solid-state batteries. Nano Energy 61:119–125

[28] Duan H, Chen W-P, Fan M, Wang W-P, Yu L, Tan S-J, Chen X, Zhang Q, Xin S, Wan L-J, Guo Y-G (2020) Building an air stable and lithium deposition regulable garnet interface from moderate-temperature conversion chemistry. Angew Chem Int Ed 59(29):12069–12075

[29] Fu K, Gong Y, Fu Z, Xie H, Yao Y, Liu B, Carter M, Wachsman E, Hu L (2017) Transient behavior of the metal interface in lithium metal-garnet batteries. Angew Chem Int Ed 56(47):14942–14947

[30] Han X, Gong Y, Fu K, He X, Hitz GT, Dai J, Pearse A, Liu B, Wang H, Rubloff G, Mo Y, Thangadurai V, Wachsman ED, Hu L (2017) Negating interfacial impedance in garnet-based solid-state Li metal batteries. Nat Mater 16(5):572–579. https://doi.org/10.1038/nmat4821

[31] Huo H, Chen Y, Li R, Zhao N, Luo J, Pereira Da Silva JG, Mücke R, Kaghazchi P, Guo X, Sun X (2020) Design of a mixed conductive garnet/Li interface for dendrite-free solid lithium metal batteries. Energ Environ Sci 13(1):127–134. https://doi.org/10.1039/C9EE01903K

[32] Duan H, Yin Y-X, Shi Y, Wang P-F, Zhang X-D, Yang C-P, Shi J-L, Wen R, Guo Y-G, Wan L-J (2018) Dendrite-Free Li-metal battery enabled by a thin asymmetric solid electrolyte with engineered layers. J Am Chem Soc 140(1):82–85. https://doi.org/10.1021/jacs.7b10864

[33] Liang J-Y, Zeng X-X, Zhang X-D, Zuo T-T, Yan M, Yin Y-X, Shi J-L, Wu X-W, Guo Y-G, Wan L-J (2019) Engineering janus interfaces of ceramic electrolyte via distinct functional polymers for stable high-voltage Li-metal batteries. J Am Chem Soc 141(23):9165–9169. https://doi.org/10.1021/jacs.9b03517

[34] Zou X, Lu Q, Zhang X, Ran R, Zhou W, Liao K, Shao Z (2020) Achieving safe and dendrite-suppressed solid-state Li batteries via a novel self-extinguished trimethyl phosphate-based wetting agent. Energy Fuels 34(9):11547–11556. https://doi.org/10.1021/acs.energyfuels.0c02222

[35] Ren YY, Liu T, Shen Y, Lin YH, Nan CW (2017) Garnet-type oxide electrolyte with novel porous-dense bilayer configuration for rechargeable all-solid-state lithium batteries. Ionics 23(9):2521–2527. https://doi.org/10.1007/s11581-017-2224-5

[36] Han FD, Yue J, Chen C, Zhao N, Fan XL, Ma ZH, Gao T, Wang F, Guo XX, Wang CS (2018) Interphase engineering

enabled all-ceramic lithium battery. Joule 2(3):497–508. https://doi.org/10.1016/j.joule.2018.02.007

[37] Du FM, Zhao N, Li YQ, Chen C, Liu ZW, Guo XX (2015) All solid state lithium batteries based on lamellar garnet-type ceramic electrolytes. J Power Sour 300:24–28. https://doi.org/10.1016/j.jpowsour.2015.09.061

[38] Munster P, Diehl M, Frerichs JE, Borner M, Hansen MR, Winter M, Niehoff P (2021) Effect of Li plating during formation of lithium ion batteries on their cycling performance and thermal safety. J Power Sour. https://doi.org/10.1016/j.jpowsour.2020.229306

[39] Wang AP, Kadam S, Li H, Shi SQ, Qi Y (2018) Review on modeling of the anode solid electrolyte interphase (SEI) for lithium-ion batteries. NPJ Comput Mater. https://doi.org/10.1038/s41524-018-0064-0

[40] An SJ, Li JL, Daniel C, Mohanty D, Nagpure S, Wood DL (2016) The state of understanding of the lithium-ion-battery graphite solid electrolyte interphase (SEI) and its relationship to formation cycling. Carbon 105:52–76. https://doi.org/10.1016/j.carbon.2016.04.008

[41] Schmitz RW, Murmann P, Schmitz R, Muller R, Kramer L, Kasnatscheew J, Isken P, Niehoff P, Nowak S, Roschenthaler GV, Ignatiev N, Sartori P, Passerini S, Kunze M, Lex-Balducci A, Schreiner C, Cekic-Laskovic I, Winter M (2014) Investigations on novel electrolytes, solvents and SEI additives for use in lithium-ion batteries: systematic electrochemical characterization and detailed analysis by spectroscopic methods. Prog Solid State Chem 42(4):65–84. https://doi.org/10.1016/j.progsolidstchem.2014.04.003

[42] Liu BY, Fu K, Gong YH, Yang CP, Yao YG, Wang YB, Wang CW, Kuang YD, Pastel G, Xie H, Wachsman ED, Hu LB (2017) Rapid thermal annealing of cathode-garnet interface toward high-temperature solid state batteries. Nano Lett 17(8):4917–4923. https://doi.org/10.1021/acs.nanolett.7b01934

[43] Du FM, Zhao N, Fang R, Cui ZH, Li YQ, Guo XX (2018) Influence of electronic conducting additives on cycle performance of garnet-based solid lithium batteries. J Inorg Mater. https://doi.org/10.15541/jim20170167

[44] Bi Y, Wang T, Liu M, Du R, Yang W, Liu Z, Peng Z, Liu Y, Wang D, Sun X (2016) Stability of Li2CO3 in cathode of lithium ion battery and its influence on electrochemical performance. RSC Adv 6(23):19233–19237. https://doi.org/10.1039/c6ra00648e

[45] Klein S, Harte P, Henschel J, Barmann P, Borzutzki K, Beuse T, Van Wickeren S, Heidrich B, Kasnatscheew J, Nowak S, Winter M, Placke T (2021) On the beneficial impact of Li2CO3 as electrolyte additive in NCM523 parallel to graphite lithium ion cells under high-voltage conditions. Adv Energy Mater. https://doi.org/10.1002/aenm.202003756

[46] Delluva AA, Kulberg-Savercool J, Holewinski A (2021) Decomposition of trace Li2CO3 during charging leads to cathode interface degradation with the solid electrolyte LLZO. Adv Funct Mater. https://doi.org/10.1002/adfm.202103716